AIAA JOURNAL
Vol. 43, No. 1, January 2005

Accuracy of the Induced Velocity from Helicoidal Vortices Using Straight-Line Segmentation

Sandeep Gupta* and J. Gordon Leishman†
University of Maryland, College Park, Maryland 20742

The accuracy of a straight-line segmentation approximation to a series of helicoidal vortices is considered. The problem is examined for different values of the helical pitch, the number of wake turns, and the wake skew angle. Results documenting both the accuracy and the relative errors of the discretized helical vortex and a vortex ring are compared. It is found that with sufficiently small segments, straight-line segmentation of both the vortex ring and of the helical vortex give at least a second-order accurate reconstruction of the induced velocity field. It is shown that the vortex ring can be viewed as a special case of a helical vortex as its pitch tends to zero. Based on the magnitude of the errors found for the two cases, a vortex ring is shown to be a more stringent test case than a helical vortex when the straight-line segmentation approach is used. The accuracy of the induced velocity field when a skewed helix is represented by straight-line segmentation is shown to be second-order accurate for various combinations of helical pitch and wake skew angle. A comparison with the unskewed helical vortex reveals that the errors in the induced velocity field are almost the same in the two cases.

Nomenclature

a	=	empirical constant for wake expansion
$\boldsymbol{E}$	=	Legendre's elliptic integral of the second kind
$\boldsymbol{K}$	=	Legendre's elliptic integral of the first kind
L_2 norm	=	second norm of the error vector
M	=	number of divisions per revolution of helical wake
N	=	number of turns in the helix
N_f	=	number of vortex filaments in the helix
p	=	helical pitch (distance between adjacent filaments normalized by radius)
R	=	rotor radius or radius of vortex ring, m
$\boldsymbol{r}$	=	position vector of vortex collocation point, m
r, θ, z	=	cylindrical polar coordinates, m, rad, m
s	=	argument in Legendre's elliptic integral
t	=	time, s
U, V, W	=	velocity components in Cartesian coordinates, ms^{-1}
U_b	=	binormal velocity, ms^{-1}
$\boldsymbol{V}$	=	velocity vector, ms^{-1}
V_{approx}	=	velocity obtained using straight-line segmentation, ms^{-1}
$\boldsymbol{V}_{\text{ex}}$	=	perturbation or external velocity vector, ms^{-1}
V_{exact}	=	exact velocity, ms^{-1}
$\boldsymbol{V}_{\text{ind}}$	=	induced velocity vector, ms^{-1}
V_r, V_θ, V_z	=	velocity components in polar coordinates, ms^{-1}
$\boldsymbol{V}_\infty$	=	freestream velocity vector, ms^{-1}
x, y, z	=	Cartesian coordinates, m
β	=	wake skew angle, deg
Γ_v	=	vortex strength (circulation), $\mathrm{m}^2\mathrm{s}^{-1}$
$\Delta\theta$	=	angular discretization of ring, rad
$\Delta\psi$	=	angular discretization of wake, rad
δ	=	cutoff angle, rad
ε_{abs}	=	absolute error
ε_{rel}	=	relative error
ζ	=	vortex wake age, rad
ψ	=	azimuthal angle, rad
Ω	=	rotational speed of turbine rotor, rad s^{-1}

Received 14 March 2003; presented as Paper 2004-0828 at the AIAA 42nd Aerospace Sciences Meeting, Reno, NV, 5–8 January 2004; revision received 14 July 2004; accepted for publication 20 July 2004.

*Graduate Research Assistant, Department of Aerospace Engineering, Glenn L. Martin Institute of Technology; sangupta@glue.umd.edu. Member AIAA.

†Minta Martin Professor, Department of Aerospace Engineering, Glenn L. Martin Institute of Technology; leishman@eng.umd.edu. Associate Fellow AIAA.

Introduction

DOWNSTREAM vortical wakes created by the rotating blades of wind turbines and other rotating-wing machines are nominally of a helicoidal form. They are usually dominated by concentrated vortices trailing from the tip of each blade. Predicting the induced-velocity field associated with the wake has been shown to be one of the key factors in improved understanding of the aerodynamics and power generation of wind turbines. The spatial and temporal geometry of the vortical wake relative to the plane of the blades varies with the turbine operating conditions, wind gradient, etc., but deviates little from the general helicoidal form. Figure 1 shows a flow visualization of the helicoidal wake structure behind a wind turbine, which was obtained in a field experiment. Notice that the wake expands downstream of the turbine and also exhibits a loss of axisymmetry, in part because of the atmospheric boundary layer and downstream shadow effect from the support tower.

Vortex methods represent the vortical structure of the wake in the form of vortex lines that exist in a potential flow. In vortex theory, the mathematical representation of the downstream wake can be done in variety of ways, such as by means of constant-vorticity straight-line filaments, curved vortex filaments, or vortex blobs.[1] The straight-line segment approximation is most often used because the induced-velocity contribution of each vortex segment can be evaluated exactly using the Biot–Savart law and involves no approximate treatment. An example is shown in Fig. 2, which is a schematic of a free-vortex wake strategy for modeling the aerodynamics of a wind-turbine wake. It will be apparent that the number of discrete vortex filaments used to approximate the wake must determine the accuracy of the reconstructed induced-velocity field. However, the computational cost for the induced-velocity calculation in the free-vortex wake method varies as the square of the number of vortex filaments. Clearly, a large number of filaments may be required for good accuracy, but gains in accuracy also have to be balanced against the higher computational costs of solving the Biot–Savart law a very large number of times.

Bhagwat and Leishman[2,3] have used an inviscid vortex ring to estimate the accuracy of a straight-line segment approximation. The induced-velocity calculations from the numerical integration of the

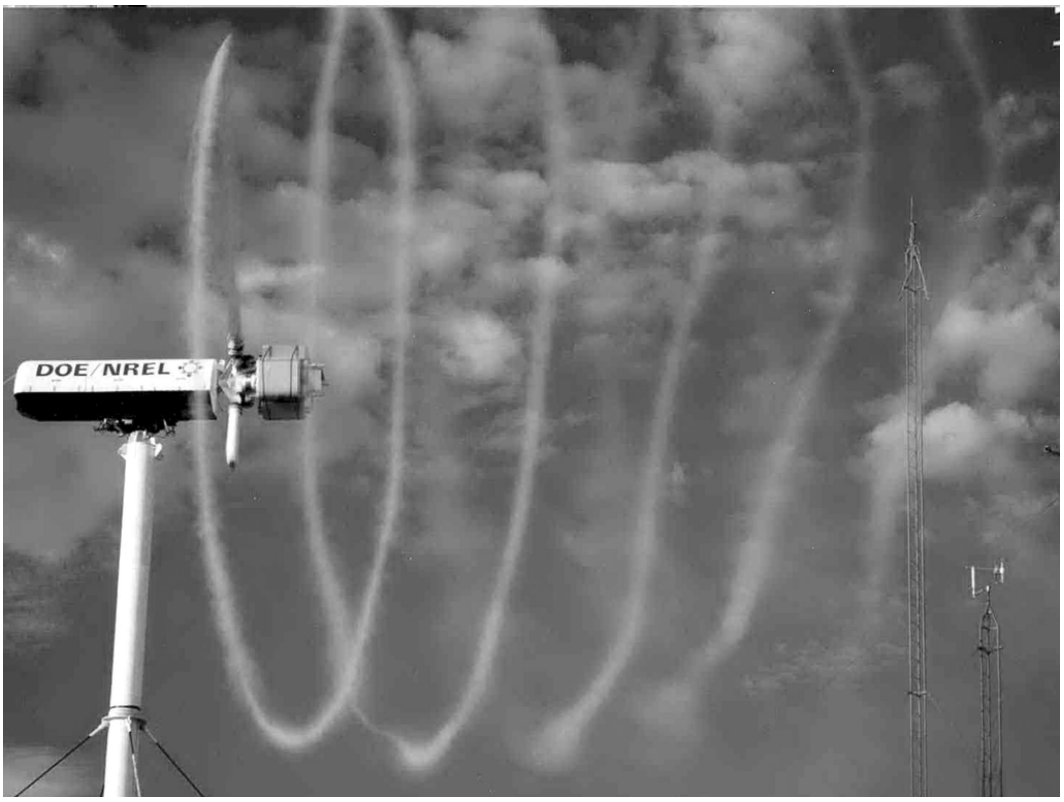

Fig. 1 Helicoidal structure of a wind-turbine wake rendered visible using smoke injection. Photo courtesy of the National Renewable Energy Laboratory.

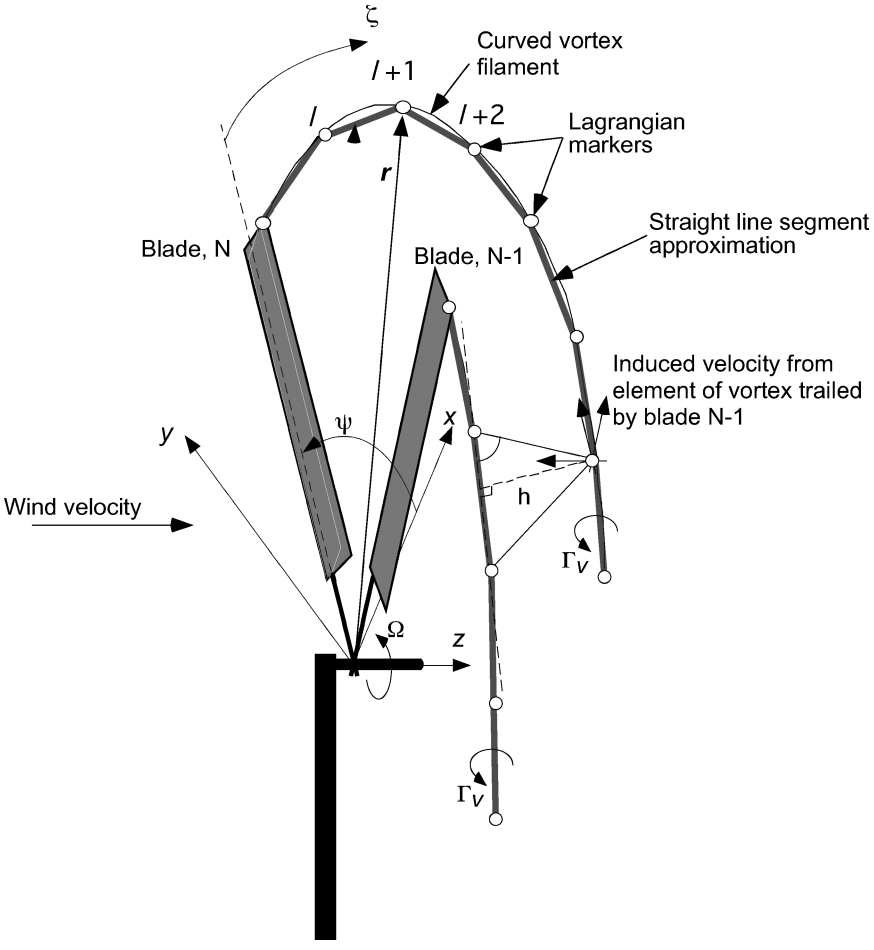

Fig. 2 Schematic of the free-vortex wake strategy for modeling the aerodynamics of wind-turbine wake.

Biot–Savart law over the ring were compared with the corresponding exact (analytical) result.[4] An error analysis was performed by calculating the L_2 norm and L_∞ norm of the relative error in the induced velocity across the plane of a vortex ring. It was shown that with appropriate levels of discretization, the straight-line segmentation can give a second-order-accurate reconstruction of the induced-velocity field.

Wood and Li[5] have suggested that a helical vortex is more appropriate and a more stringent case for estimating the accuracy of the straight-line segmentation approach in reconstructing the velocity field. Three test cases for various helical-pitch values of a helical vortex were considered. These authors showed second-order accuracy for a control point away from the filament and a dependence on the helical pitch for control points near the singularity on the vortex axis. Asymptotic results for the binormal velocity of a singly infinite helical vortex (as derived by Boersma and Wood[6,7]) were used where an analytic solution was not available. Wood and Li also argued that a vortex ring is not a special case of a helical vortex when its helical pitch tends to zero, a result that is at variance with the observations made in the present work.

For the aerodynamic analysis of wind turbines using vortex methods, there is a need to carefully evaluate the accuracy of the straight-line segmentation approach to the downstream vortex wake and to establish thresholds of discretization that will provide good accuracy although still containing computational costs. Therefore, the objective of the present work is to estimate the net accuracy of the velocity field that is induced by helical vortices using a straight-line segmentation approximation and to provide general guidance in establishing acceptable levels of discretization in free-vortex wake schemes. Notice that this study is also relevant to helicopter-rotor-wake modeling using vortex methods.[8]

First, the induced velocity distribution and the error behavior of a vortex ring and a helical vortex are compared with each other. The results examine the error behavior with respect to the exact solution for the velocity that is induced by a vortex ring and the numerical results that are found using the finest grid discretization for the helical vortex. A helical vortex or a singly infinite helical vortex is represented by a finite number of turns for the induced-velocity reconstruction using the vortex method. The velocity induced by a vortex ring is then compared to the result for helical vortices with small values of pitch. It is shown that the induced velocity from a helical vortex can be viewed to reduce to the case of a vortex ring for values of the helical pitch approaching zero. The order of accuracy of the induced-velocity reconstruction by means of straight-line segmentation of a helical vortex is then discussed and is compared to results for different levels of discretization and numbers of turns of the helix. Finally, the case of a skewed helical vortex is analyzed, which is representative of the downstream wake produced by a wind turbine when it is yawed with respect to the oncoming wind.

Methodology

Over the past few decades, vortex methods have emerged as robust tools for modeling the aerodynamics and wake dynamics of rotating wings (see Ref. 8 for a review). Vortex-wake methods can be broadly classified into two categories, namely prescribed-vortex-wake methods and free-vortex-wake methods. In a prescribed-wake analysis, the geometry of the wake downstream of the rotor disk is specified a priori based on certain semi-empirical rules.[9–11] In the free-vortex-wake analysis, which is much less well developed or validated for wind-turbine applications, the wake is allowed to develop naturally to force-free positions. In either case, the vortex-wake approach is based on the assumptions of potential flow, with all of the vorticity being assumed to be confined inside a finite number of vortex filaments. Lagrangian markers placed on the vortex filaments are linked together, and these markers and the associated vorticity are then convected naturally through the flow field at the local flow velocity.

Using the principles of vorticity transport, the convection of the Lagrangian markers on a free vortex filament is described by the equation[8]

$$\frac{\mathrm{d}\boldsymbol{r}}{\mathrm{d}t} = \boldsymbol{V}(\boldsymbol{r}, t) \tag{1}$$

In Eq. (1), $\boldsymbol{r}$ is the position vector of the marker lying on a vortex filament (Fig. 2) and $\boldsymbol{V}$ is the local velocity of that marker. In blade-fixed coordinates, this equation can be written as the partial differential equation

$$\frac{\partial \boldsymbol{r}}{\partial \psi} + \frac{\partial \boldsymbol{r}}{\partial \zeta} = \frac{\boldsymbol{V}(\boldsymbol{r})}{\Omega} \tag{2}$$

where ψ is the azimuthal position of a blade defined from a reference datum and ζ is the time (age) of the vortex filament since it was trailed into the flow (Fig. 2). The left-hand side of the foregoing equation is essentially a one-dimensional wave equation. The equation is solved numerically using finite difference approximations by discretizing the domain into steps of $\Delta\psi$ and $\Delta\zeta$. The discretized equation is written as

$$(D_\psi + D_\zeta)\boldsymbol{r} = \frac{1}{\Omega}\sum \boldsymbol{V} \tag{3}$$

where D_ψ and D_ζ denote the finite difference approximations to the first derivatives. The velocity term on the right-hand side is the sum of the freestream velocity $\boldsymbol{V}_\infty$, any external sources of perturbation $\boldsymbol{V}_{\mathrm{ex}}$, such as the atmospheric boundary layer, wind turbulence, etc., and the wake induced velocity $\boldsymbol{V}_{\mathrm{ind}}$ (Ref. 12). Therefore, $\boldsymbol{V}$ can be written as

$$\boldsymbol{V} = \boldsymbol{V}_\infty + \boldsymbol{V}_{\mathrm{ex}} + \boldsymbol{V}_{\mathrm{ind}} \tag{4}$$

The left-hand side of the wake equations can be solved by a variety of finite difference methods of any order. A study on the accuracy and stability of the various time-marching schemes used in the time-marching free-vortex wake methods has been done by Bhagwat and Leishman[2] and Gupta and Leishman.[13] The overall accuracy of the numerical scheme is, however, determined by the lowest order accurate term. It is the right-hand side of Eq. (3) and the accuracy of the subsequent velocity field reconstruction that are of primary interest in the present work. The wake induced velocity V_{ind} is a highly nonlinear term and it is the most difficult and expensive contributing element of the wake problem to calculate accurately. The solution to the wake induced velocity is evaluated by the application of the Biot–Savart law as an integral along the complete length of each vortex wake filament. This integral is, in general, not available in analytic form for curvilinear vortex filaments. To overcome this, straight-line segmentation of the vortex filament is the most natural and also because the exact solution to the induced-velocity contribution for each segment can be found.

Consider a vortex segment of infinitesimal length $\mathrm{d}\boldsymbol{l}$ and a point P at a distance $\boldsymbol{r}$ from a line segment AB. By means of the Biot–Savart law, the velocity $\mathrm{d}\boldsymbol{V}$ that is induced at point P by the vortex segment is given by

$$\mathrm{d}\boldsymbol{V} = (\Gamma_v/4\pi)[(\mathrm{d}\boldsymbol{l} \times \boldsymbol{r})/|\boldsymbol{r}|^3] \tag{5}$$

For a finite segment, where $\boldsymbol{r}_1$ and $\boldsymbol{r}_2$ are the distances of the end point of the line segment from a point P, the induced velocity $\mathrm{d}\boldsymbol{V}$ can be written as[14]

$$\mathrm{d}\boldsymbol{V} = (\Gamma_v/4\pi)(\boldsymbol{r}_1 \times \boldsymbol{r}_2)(1/r_1 + 1/r_2)[1/(r_1 r_2 + \boldsymbol{r}_1 \cdot \boldsymbol{r}_2)] \tag{6}$$

One of the disadvantages of all types of vortex methods is the relatively large number of individual vortex filaments necessary to fully resolve the vortical flow and the associated high computational cost of evaluating the Biot–Savart law for each and every filament. The cost of induced-velocity reconstruction in a free-vortex wake method varies as the square of the number of vortex elements N_f. This often prevents the use of very fine discretization in the free-vortex wake calculations, and the practical range of azimuthal discretization is usually between $\Delta\psi = 5$ deg and $\Delta\psi = 20$ deg. Unfortunately, the use of larger segments can compromise the accuracy of

the induced-velocity-field reconstruction. Therefore, there is a need to carefully evaluate the accuracy of the straight-line-segmentation approach and to establish thresholds of discretization that will provide good accuracy although still containing computational costs.

Results and Discussion

The geometry of the wind-turbine wakes varies with operating conditions, wind direction, and atmospheric turbulence but is of a nominally helicoidal form. To analyze the overall accuracy of the straight-line vortex segmentation approach, idealized wake geometries are considered. Using a "real" wake will modify only the magnitude of errors and not the overall accuracy. A vortex ring is considered first because an exact solution for the velocity that is induced by a vortex ring is available. To understand the effect of the variation of the wind velocity and yawed flow on the accuracy of induced-velocity reconstruction, a helical vortex (represented by a finite number of turns) with different helical pitch values and skew angles is used. The effect of the expansion of the wake behind a wind turbine on the accuracy of the straight-line segmentation is also investigated.

Vortex Ring

A vortex ring can be thought of as one revolution of the helicoidal wake with the helical pitch equal to zero. Figure 3 shows a schematic of a vortex ring that is discretized into straight-line segments. The sum of the induced velocity from each vortex segment, which is performed using numerical integration with the Biot–Savart law, gives an approximation to the velocity that is induced by the vortex ring at any point in the flowfield.

The exact solution for the velocity that is induced by a vortex ring is given by the integration of Eq. (6) over the perimeter of the ring, which is given in polar coordinates r and z by

$$V_r(r,z) = -\frac{\Gamma_v}{4\pi}\int_{\delta}^{2\pi-\delta} \frac{Rz\cos\theta}{(R^2+r^2-2rR\cos\theta+z^2)^{\frac{3}{2}}}\,\mathrm{d}\theta$$

$$V_z(r,z) = -\frac{\Gamma_v}{4\pi}\int_{\delta}^{2\pi-\delta} \frac{R(R-r\cos\theta)}{(R^2+r^2-2rR\cos\theta+z^2)^{\frac{3}{2}}}\,\mathrm{d}\theta \quad (7)$$

Here δ is the cutoff angle, which can be set equal to the angular discretization of the vortex ring.

An exact solution for the velocity that is induced by a vortex ring at any point can be found in terms of elliptic integrals.[4] For a vortex ring with strength $\boldsymbol{\Gamma}_v$ and radius R, the axial and radial velocity components are given by

$$V_z(r,z) = \frac{-\Gamma_v}{2\pi\sqrt{z^2+(r+R)^2}}\left[\boldsymbol{K}(s)+\frac{R^2-r^2-z^2}{z^2+(R-r)^2}\boldsymbol{E}(s)\right]$$

$$V_r(r,z) = \frac{-\Gamma_v z}{2\pi\sqrt{z^2+(r+R)^2}}\left[\boldsymbol{K}(s)-\frac{R^2+r^2+z^2}{z^2+(R-r)^2}\boldsymbol{E}(s)\right] \quad (8)$$

respectively, where $\boldsymbol{K}(s)$ and $\boldsymbol{E}(s)$ are elliptic integrals of the first and second kind, respectively. The argument s is defined by the equation

$$s = \sqrt{\frac{4rR}{z^2+(r+1)^2}} \quad (9)$$

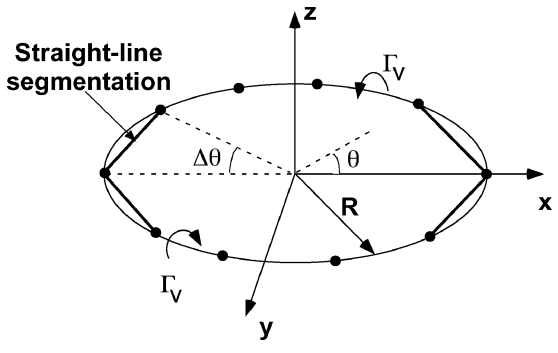

Fig. 3 Schematic of a vortex ring discretized by straight-line segments.

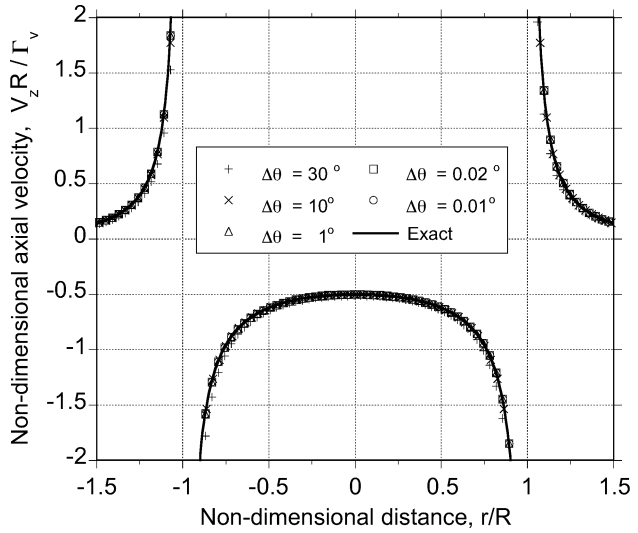

Fig. 4 Induced velocity in the plane of a vortex ring for different levels of straight-line segmentation.

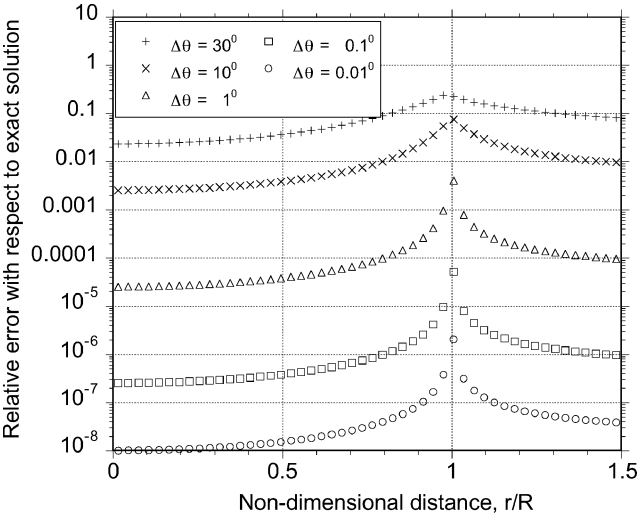

Fig. 5 Numerical error distribution in the vortex-ring plane for different levels of straight-line segmentation.

The velocity induced by the discretized vortex ring was calculated along a diameter across the plane of the vortex ring. All of the calculations were done using double-precision arithmetic. In the plane of the vortex ring, the radial component of the induced velocity is zero and only the axial component exists. The azimuthal discretization level was varied from a relatively coarse azimuthal segmentation of $\Delta\psi = \Delta\theta = 30$ deg to a fine resolution of $\Delta\psi = \Delta\theta = 0.01$ deg.

Figure 4 shows the numerical results for the axial component of the induced velocity, V_z, for various discretization levels, as compared to the exact solution given by Eq. (8). The exact solution is not defined at $r/R = 1$, where a logarithmic singularity exists. For all other points in the plane of the ring, the numerical results showed good agreement with the exact solution. For the case where $\Delta\theta = 0.01$ deg, the two values were found to agree numerically at up to seven decimal places. Figure 5 shows the relative error distribution along the radius of the vortex ring. The magnitude of the relative error was found to be at a maximum near the singularity at $r/R = 1$ and then it decreased away from the singularity.

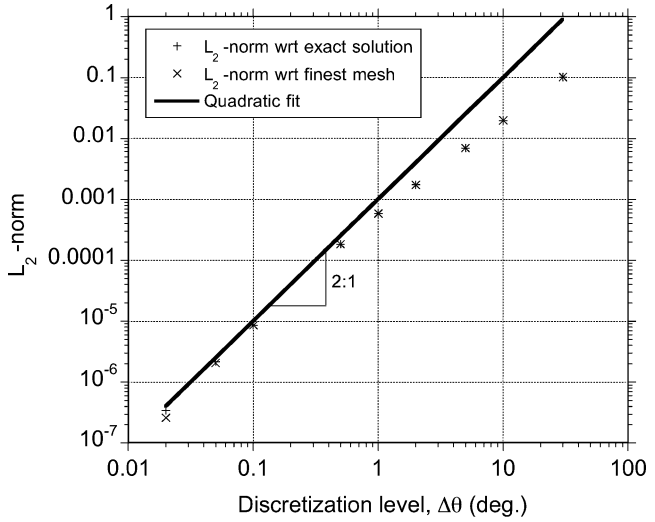

Fig. 6 L_2 norm vs discretization for a vortex ring showing second-order accuracy.

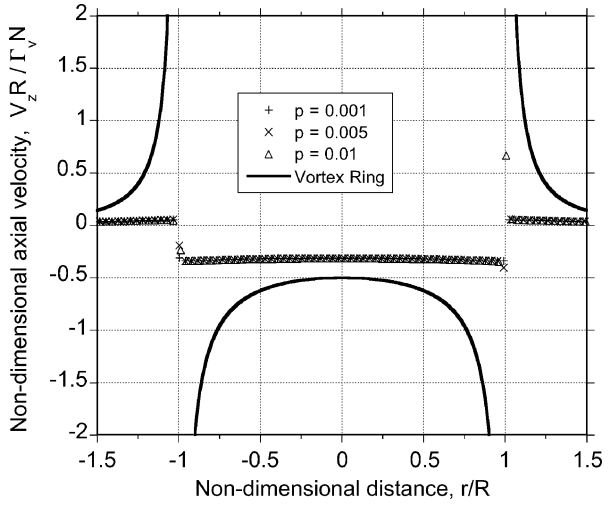

Fig. 7 Induced-velocity distribution from a helical vortex for decreasing helical pitch with $N \times p$ constant. An azimuthal discretization of $\Delta\theta = 0.1$ deg is used. The exact velocity induced by a vortex ring is also shown.

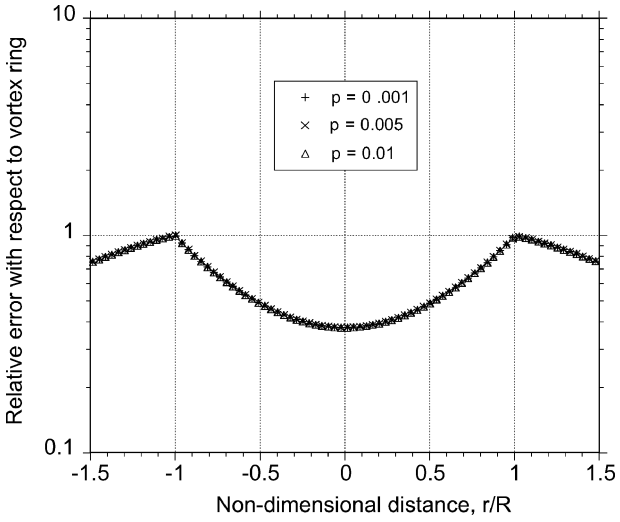

Fig. 8 Error distribution in induced velocity from a helical vortex for decreasing helical pitch with $N \times p$ constant compared to a vortex ring. An azimuthal discretization of $\Delta\theta = 0.1$ deg is used.

To estimate the overall net accuracy of the reconstruction of induced velocity from the vortex ring, a plot of L_2 norm vs discretization level is shown in Fig. 6. In the first case, the error was calculated with respect to the exact solution, and in the second case, it was calculated with respect to the numerical solution from the finest level of discretization ($\Delta\theta = 0.01$ deg). The results essentially coincide for all discretization levels. A quadratic fit to the results is also shown, indicating clean second-order accuracy. For coarse discretizations, say $\Delta\theta > 10$ deg, the maximum error increases to more than 10%, and the order of accuracy also appears to be somewhat lower. These results show that for reasonably fine wake discretizations, the induced-velocity calculation is at least second-order accurate. Furthermore, because the induced-velocity calculation from the finest discretization compares so well with the exact solution, this observation will be used in the analysis of helical vortices, for which an analytic solution to the induced-velocity field cannot be found.

Comparison of a Vortex Ring and a Helical Vortex

A vortex ring can be thought of as one revolution of a wind-turbine wake with a helical pitch that approaches zero. However, it has been argued by Wood and Li[5] that the vortex ring is not a special case of a helical vortex with helical pitch $p \to 0$. Also, they have argued that a helical vortex is a more stringent case to determine the accuracy of the straight-line segmentation approach.

To better understand this problem and to compare the two cases quantitatively, the induced-velocity distribution of a singly infinite helical vortex with very small helical pitch was examined and compared to that of a vortex ring. The induced velocities were normalized by the number of wake turns. Three cases were considered: 1) Spatial extent of the helical vortex $N \times p$ was held constant. 2) Number of turns in the helix N for different values of helical pitch p was held constant. 3) Number of turns of the helix was varied for a constant helical pitch p. In each case, the results will be shown for an azimuthal discretization of $\Delta\theta = 0.1$ deg. It was shown previously that the numerical evaluation of the Biot–Savart using an azimuthal discretization of $\Delta\theta = 0.1$ deg to obtain the induced-velocity field gives a maximum error of less than 0.01%, which is essentially exact for any practical purpose.

1) Case 1: $N \times p$ is constant. In this case, the spatial extent of the helical vortex was kept constant. For $p = 0.01$, a total of 20 turns were used for the helical vortices. For decreasing helical pitch, the number of turns was increased to keep the product $N \times p =$ constant, and hence the spatial extent of the helix was kept constant.

Figure 7 shows the induced-velocity distribution across the $z = 0$ plane for the helical vortex. Notice that the induced velocity is scaled by the number of turns. Also shown for reference is the induced-velocity distribution from a vortex ring across the same plane. With decreasing helical pitch, the induced-velocity distribution remains the same and clearly does not approach the induced-velocity distribution from a vortex ring. Figure 8 shows the error distribution of the induced velocity as compared to the exact solution for a vortex ring. An azimuthal discretization of $\Delta\theta = 0.1$ deg is used. For various helical-pitch values, the error distribution was found to be the same.

2) Case 2: Constant N. For the second case the number of turns of the helical vortex was kept constant for different helical-pitch values and so the spatial extent of the helical vortex decreased with decreasing pitch. A total of 20 turns were used to model the helical vortices.

The induced-velocity distribution for the helical vortex is shown in Fig. 9. In this case, with decreasing helical pitch the induced-velocity distribution was found to approach the velocity distribution from the vortex ring, as shown by the solid line. Figure 10 shows the magnitude of the error in the induced velocity calculated with respect to the induced velocity from a vortex ring. The magnitude of this error was found to decrease as the helical pitch decreased.

3) Case 3: Constant p. The variation in the induced-velocity distribution for a fixed helical pitch p but for an increasing number of turns was also studied. Figure 11 shows the induced-velocity

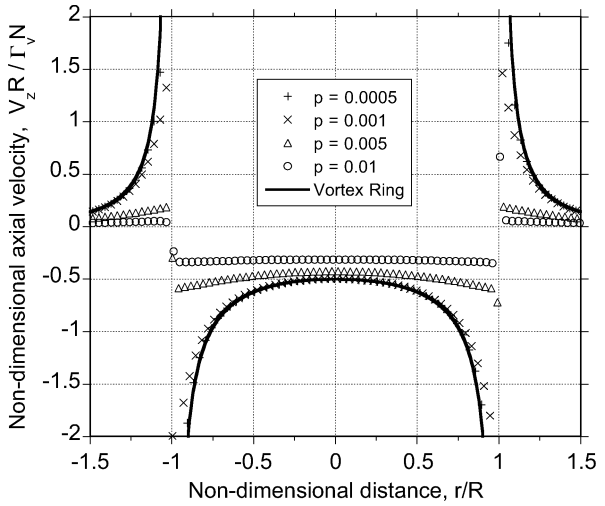

Fig. 9 Induced-velocity distribution from a helical vortex for decreasing helical pitch with N constant. An azimuthal discretization of $\Delta\theta = 0.1$ deg is used. The exact velocity induced by a vortex ring is also shown.

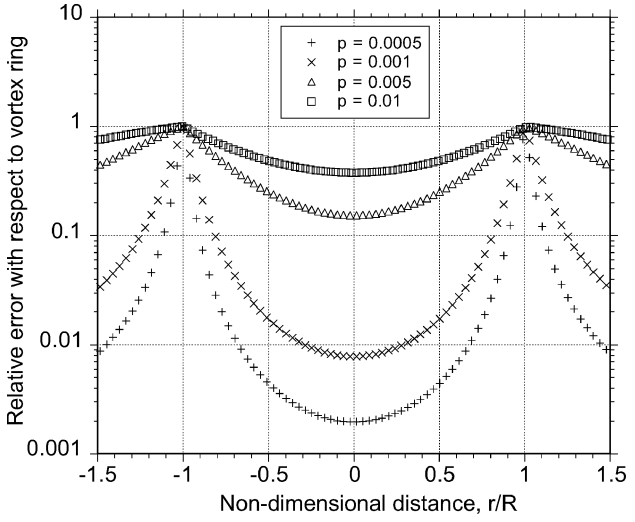

Fig. 10 Error distribution in induced velocity from a helical vortex for decreasing helical pitch with N constant, compared to a vortex ring. An azimuthal discretization of $\Delta\theta = 0.1$ deg is used.

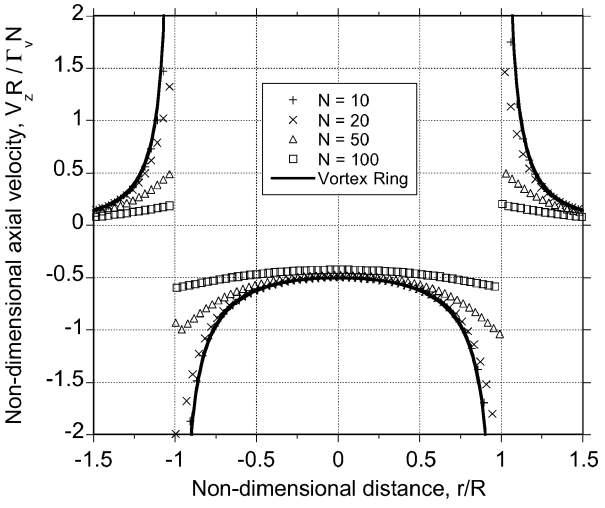

Fig. 11 Induced-velocity distribution from a helical vortex for increasing number of turns and constant helical pitch $p = 0.001$. An azimuthal discretization of $\Delta\theta = 0.1$ deg is used. The velocity induced by a vortex ring is also shown.

distribution from the helical vortex with $p = 0.001$ for increasing N. It can be seen that the velocity distribution differs more and more from the vortex-ring case as N is increased.

In summary, these results show that a helical vortex reduces to a vortex ring as the helical pitch $p \to 0$ provided the number of turns N is kept constant. If the spatial extent of the helical vortex is kept constant, then the velocity distribution does not depend on the helical pitch. When the helical pitch is reduced for a constant N, the case of a vortex ring is approached. If the number of turns is increased for small but finite helical pitch (Fig. 11), then the induced-velocity distribution becomes less like the vortex-ring case.

Accuracy of Straight-Line Segmentation to a Helical Vortex

In the preceding section, the induced-velocity distribution and errors for a helical vortex with very small pitch were compared with those of a vortex ring. The vortex ring has been established as a special case of helical vortex with the helical pitch tending to zero but only if the number of turns is held constant and is finite. In the present section, the accuracy of the induced-velocity reconstruction from a helical vortex will be considered.

It was shown previously that the induced-velocity results from the finest discretization of the vortex ring agreed very well with the exact solution. Because an exact solution for the helical vortex is not available, the result for the finest grid resolution will be used to assess the accuracy of the induced velocity from the helical vortex (i.e., the errors were calculated with respect to the numerical results from the finest discretization level). Results were studied for a range of values of helical pitch p and 20 turns were used to represent the helical vortex. All the calculations were performed using double-precision arithmetic. The relative error is defined as

$$\varepsilon_{\text{rel}} = (V_{\text{approx}} - V_{\text{exact}})/V_{\text{exact}} \tag{10}$$

Figure 12 shows the induced velocity from a helical vortex with a helical pitch of $p = 0.05$. Notice that although r has been defined as the radial position and is nonnegative, r/R has been used as the nondimensional radius with sign. The induced-velocity distribution has a singularity at $r/R = +1$, but the variation near $r/R = -1$ is much smoother. The error distribution in the induced velocity calculated with respect to the finest grid discretization is shown in Fig. 13. This error distribution shows a maximum at $r/R = -1.2$ and a minimum at $r/R = -0.7$. The induced velocity near $r/R = -1.2$ is close to zero, which causes an increase in the relative error near this point. The maximum error still occurs at the singularity (at $r/R = 1$). The solid line is provided as a reference and shows the relative error in the induced velocity for a vortex ring for a discretization of $\Delta\theta = 0.02$ deg with respect to the finest discretization. It can be seen that at most of the points, the magnitude of the relative error

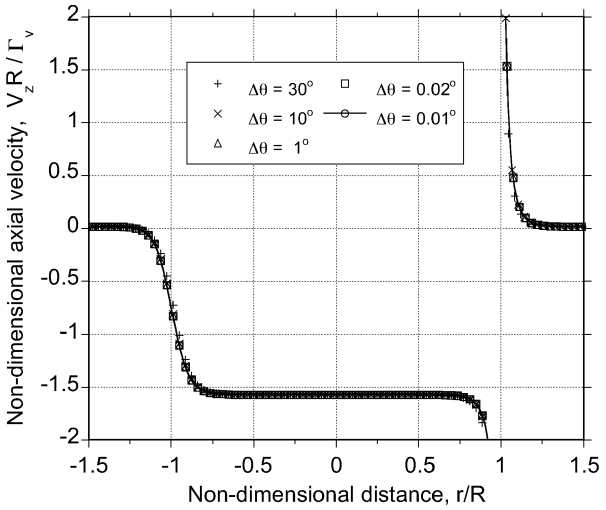

Fig. 12 Induced velocity in the $z = 0$ plane of a helical vortex with pitch $p = 0.05$ calculated using straight-line segmentation.

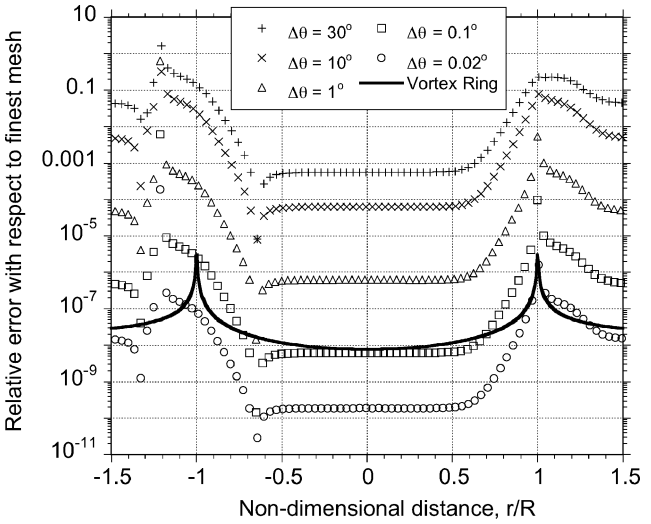

Fig. 13 Error distribution in the induced velocity in the $z = 0$ plane of a helical vortex ($p = 0.05$) with respect to the finest discretization. Error distribution for the case of a vortex ring ($\Delta\theta = 0.02$ deg) with respect to the finest discretization is also shown.

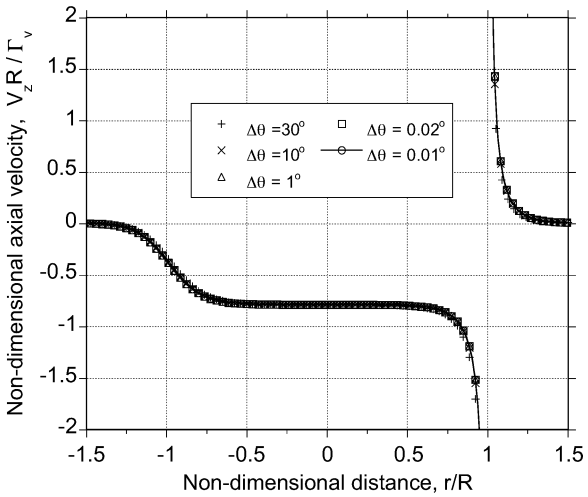

Fig. 14 Induced velocity in the $z = 0$ plane of a helical vortex with pitch $p = 0.1$ calculated using straight-line segmentation.

for the vortex ring is greater than that for the helical vortex with the same discretization. The position of the minimum error is governed by the self-cancellation of errors resulting from successive turns of the helix.

Figure 14 shows the velocity distribution for a helical vortex with a pitch of $p = 0.1$. The velocity distribution was found to be essentially the same as in the previous case, except for the value of the constant velocity near $r/R = 0$. The error distribution (Fig. 15) has only one minimum at $r/R = -0.2$ and a maximum exists near the singularity at $r/R = 1.0$.

Figure 16 shows the L_2 norm error in the induced-velocity field versus the discretization level for various values of the helical pitch. A curve fit is also shown to bring out the nature of the numerical errors. For all values of helical pitch, the errors were noticed to decrease quadratically with grid refinement. The results were similar to those found for the vortex ring, as discussed previously. The magnitude of the L_2 norm (computed from the relative error) for $p = 0.05$ was found to be greater than in the other cases because the induced velocity for this case is close to zero at some control points, which pushes up the relative error. The accuracy was less than second-order for coarse discretizations and, as found for the vortex-ring case, a discretization of at least $\Delta\theta = 10$ deg was required to keep the maximum error in the induced-velocity field less than 10%.

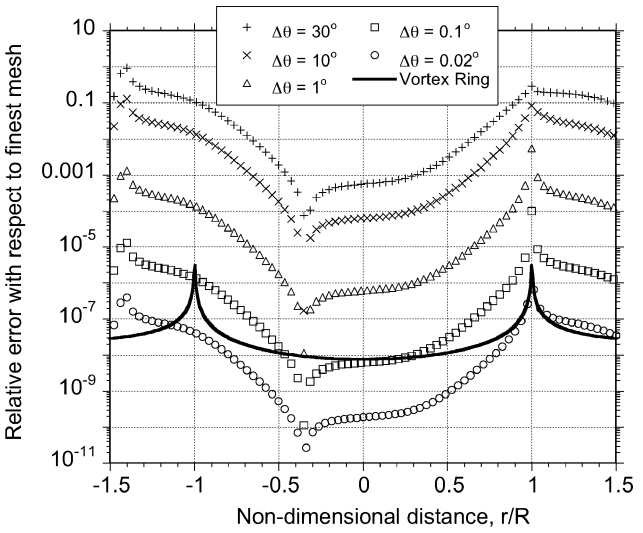

Fig. 15 Error distribution in the induced velocity $z = 0$ plane of a helical vortex ($p = 0.1$) with respect to the finest discretization. Error distribution for the case of a vortex ring ($\Delta\theta = 0.02$ deg) with respect to the finest discretization is also shown.

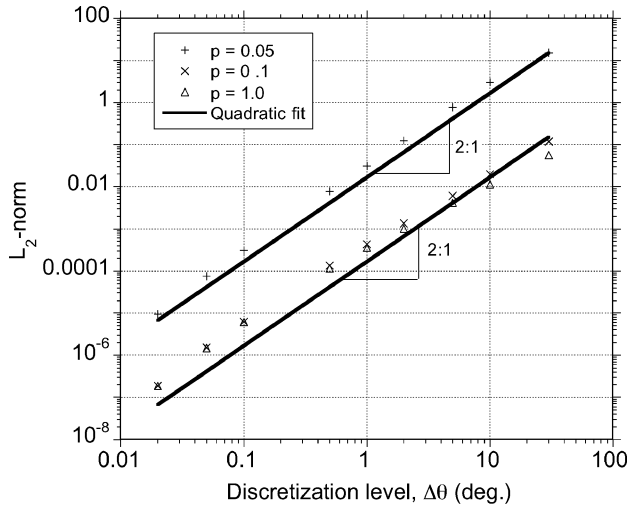

Fig. 16 L_2 norm vs discretization level for various pitch values showing the convergence trend for the numerical scheme for the accuracy of induced-velocity calculation by straight-line segmentation of a helical vortex.

Expanding Helical Wake

An asymptotic model for the expanding wake given by Wood[15] has been used to study the accuracy of induced-velocity reconstruction for an expanding helical vortex. The wake expands for the first five revolutions and has a constant radius thereafter as given by

$$r(\theta) = \begin{cases} R(a\theta + 1), & \theta < 10\pi \\ R(a10\pi + 1), & \theta \geq 10\pi \end{cases} \tag{11}$$

Here $a = 0.035$ is an empirical constant obtained from Ref. 15. Figure 17 shows the L_2 norm error in the induced-velocity field versus the discretization level for two values of the helical pitch for an expanding helical wake. It is clear from Fig. 17 that the inclusion of expansion in the helical wake does not change the second-order-accurate behavior of induced-velocity reconstruction using straight-line vortex segmentation.

Comparison with Results of Wood and Li

In this section, the accuracy of the reconstruction of the induced-velocity field from a helical vortex using straight-line segmentation is considered. The approach follows the procedure of Wood and Li.[5]

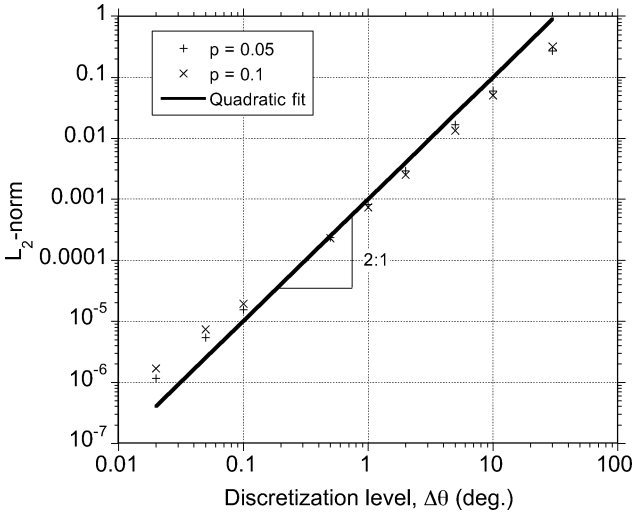

Fig. 17 L_2 norm vs discretization level for various pitch values showing the convergence trend for the straight-line segmentation of an expanding helical vortex.

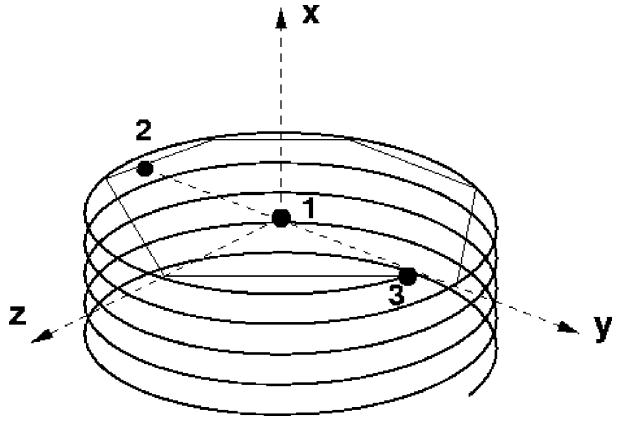

Fig. 18 Schematic of a helical vortex discretized by straight-line segments, showing the three control points (from Ref. 5).

Three cases were considered, as shown in Fig. 18. In the first case, the induced velocity on the axis of the helix at point 1: $(x, y, z = 0, 0, 0)$ was considered, for which an analytic solution is available. The second case considered was point 2: $(x, y, z = 0, -1, 0)$, which is at the same radius as the vortex but displaced from the vortex axis by a distance, $pR\pi$. The third case considers the self-induced velocity at point 3: $(x, y, z = 0, 1, 0)$. Note that in this section the x axis corresponds to the axial direction consistent with the convention used in Ref. 5.

An exact solution $U = p^{-1}$ is available for point 1. For points 2 and 3, a binormal velocity is available from the analysis given in Refs. 6 and 7, which was obtained using asymptotic expansions for small and large pitch of the helix. The results for the binormal velocity from Boersma and Wood[6,7] are given up to six significant figures for all values of helical pitch. In the present study, the binormal velocity was calculated numerically using the direct application of the Biot–Savart law. The error behavior with respect to the exact solution for point 1 and the binormal velocity given in Table 1 in Wood and Li[5] for points 2 and 3 is compared with that of Ref. 5 for a wide range of helical-pitch values. The binormal velocity U_b is calculated from the x and z direction velocities U and W by means of

$$U_b = (U \pm pW)/(p^2 + 1)^{\frac{1}{2}} \tag{12}$$

where pW is added for point 2 and subtracted for point 3. The components U and W are the sum of the induced velocities contributed from each straight-line segment as obtained by the Biot–Savart law.

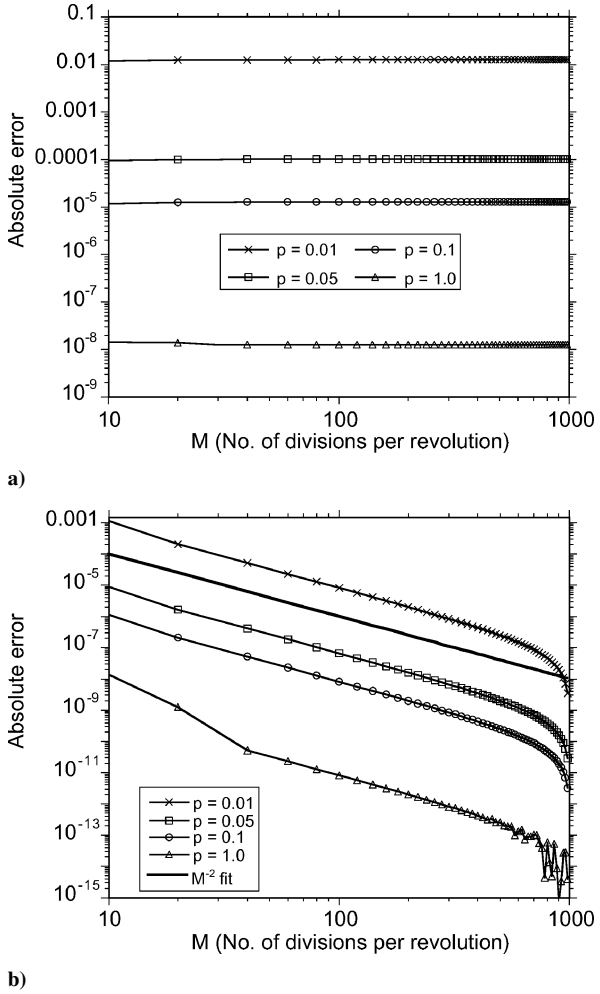

Fig. 19 Absolute error in the induced velocity for case 1 with respect to a) the exact solution $1/p$ and b) the induced velocity for the finest discretization of a helical vortex.

In the first method, the helical vortex was approximated by a large number of helical turns (1000 turns was found to be acceptable to reduce the contribution of the "analytic remainder"), which was held constant for different discretization levels. This is different from the procedure of Wood and Li, which will be analyzed later. The analytic remainder, which approximates the remaining contribution from the indefinite integral, was not calculated; according to Wood and Li[5] this analytic remainder does not contribute significantly to the calculation of the induced velocities.

Figure 19 shows the absolute error plotted against the discretization level for point 1 with respect to the analytical solution and the finest discretization solution. This figure corresponds to Fig. 4 in Wood and Li.[5] The error with respect to the analytical solution for a particular value of helical pitch was noted to stay constant and was not sensitive to the discretization level. However, the error variation with respect to the finest discretization shows a second-order behavior. The fluctuations in the error variation at higher M for $p = 1.0$ (see Fig. 19b) are because of the precision errors.

The variation of absolute error with discretization level for point 2 is shown in Fig. 20. The dashed line shown a quadratic fit (a M^{-2} fit), indicating that the accuracy of the induced velocity reconstruction for point 2 is second order and does not change for large values of M. The increase in the error for large M for $p = 0.05$ and $p = 0.1$, which was shown in Ref. 5, was not found from the results computed here. The variation of the error with respect to the analytical solution and the finest discretization solution shows a similar behavior.

Figure 21 shows the error variation for point 3. The cutoff method of Saffman[16] was used to exclude the logarithmic singularity at this point. For small values of helical pitch ($p = 0.01$ and $p = 0.05$), the absolute error with respect to analytical solution was found to

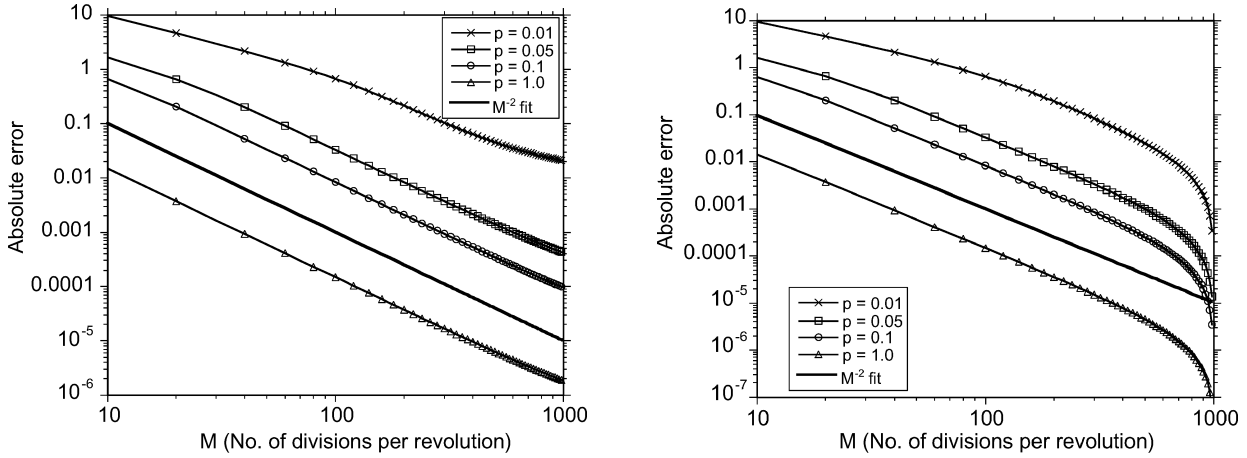

Fig. 20 Absolute error in the induced velocity for case 2 with respect to a) the binormal velocity U_b given in Table 1 in Ref. 5 and b) the binormal velocity for the finest discretization.

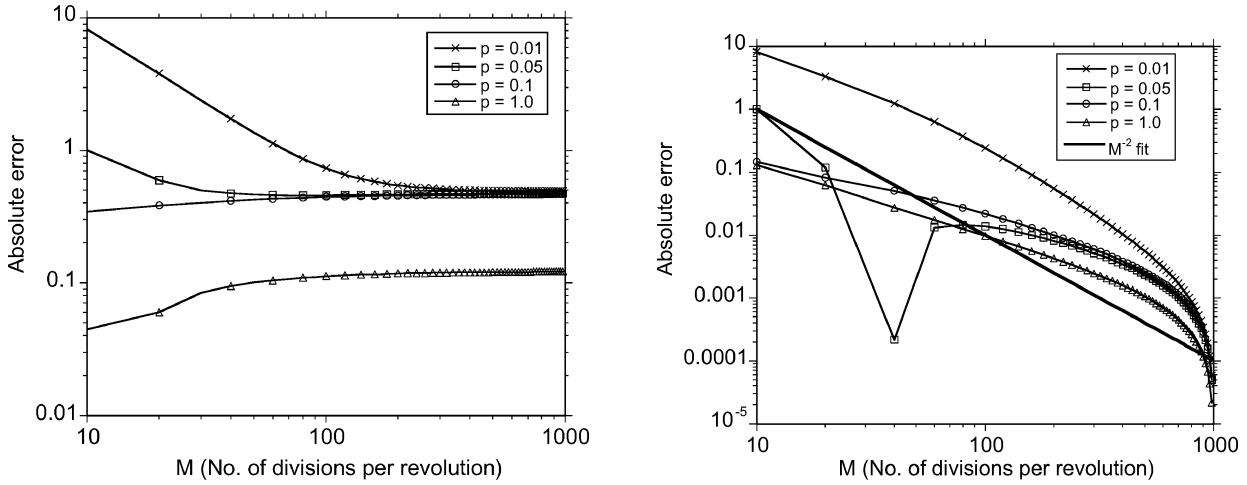

Fig. 21 Absolute error in the induced velocity for case 3 with respect to a) the binormal velocity U_b given in Table 1 in Ref. 5 and b) the binormal velocity for the finest discretization.

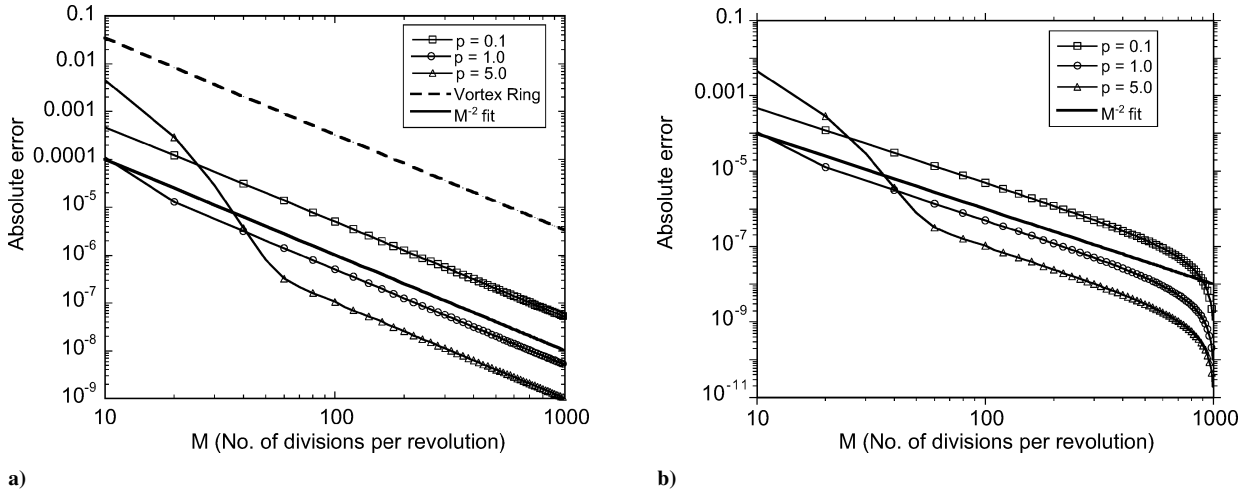

Fig. 22 Absolute error in the induced velocity for case 1 with respect to a) the exact solution 1/p and b) the induced velocity for the finest discretization.

decrease with increasing discretization level. For higher values of helical pitch, the absolute error increased with increasing values of M. This variation is consistent with the results shown in Fig. 6a of Ref. 5. The error variation with respect to best solution shows a less than second-order-accurate trend. These results show that the "analytic remainder" introduces a significant error and dominates the error behavior in case 1 but does not affect the error behavior for cases 2 and 3.

The second method, as proposed by Wood and Li,[5] approximates the helical vortex with a finite number of number of turns, depending upon the number of divisions per revolution (M or the discretization level) and the helical pitch. In this case the number of turns is

$$N = 5M/\pi p \tag{13}$$

An error analysis using this value of N was performed for the three control points. As shown in Figs. 22 and 23, this approach gives a

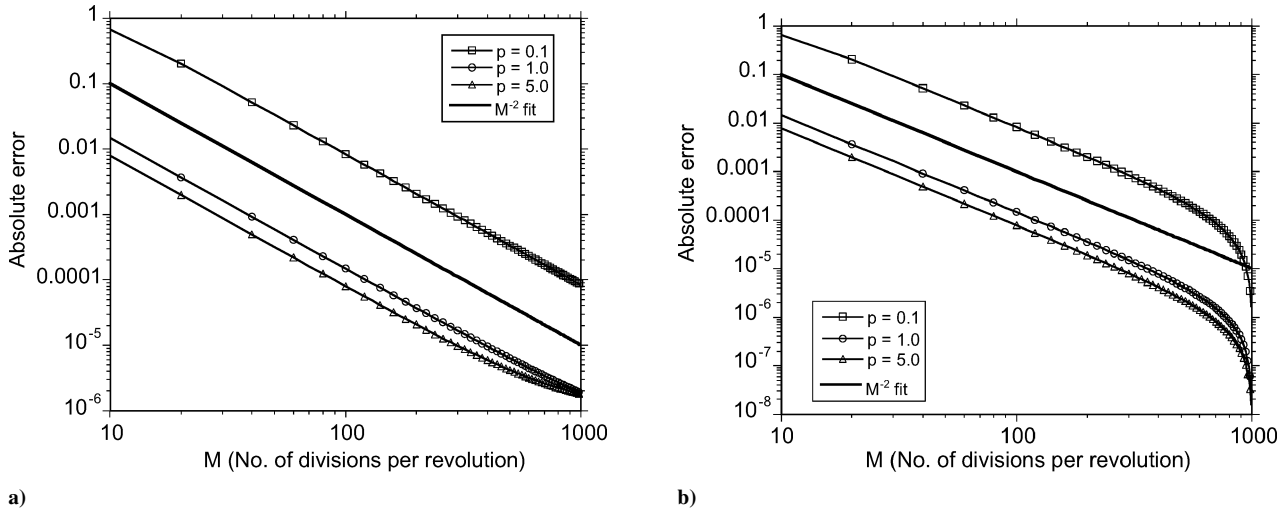

Fig. 23 Absolute error in the induced velocity for case 2 with respect to a) the binormal velocity U_b given in Table 1 in Ref. 5 and b) the binormal velocity for the finest discretization. The number of turns is given by Eq. (13).

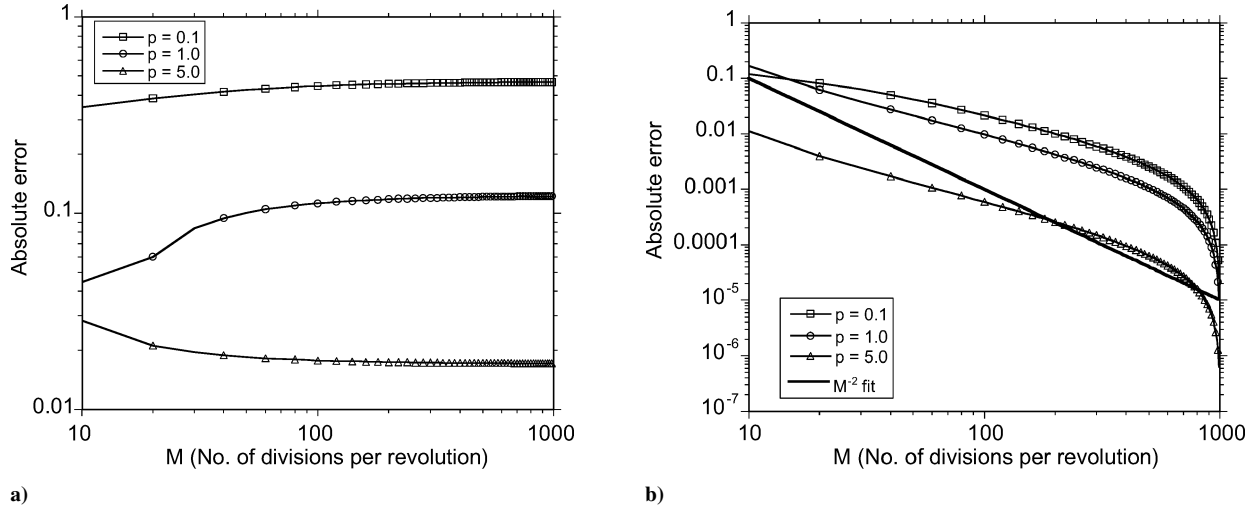

Fig. 24 Absolute error in the induced velocity for case 3 with respect to a) the binormal velocity U_b given in Table 1 in Ref. 5 and b) the binormal velocity for the finest discretization. The number of turns is given by Eq. (13).

second-order trend for the variation of the error at points 1 and 2 with respect to the analytical solution and finest discretization solution. Results for small helical pitch ($p = 0.01$ and $p = 0.05$) are not shown because of the large number of turns required according to Eq. (13), yet the results shown in Fig. 22 are in very good agreement with Fig. 4 of Ref. 5. The solid line shows a M^{-2} fit, indicating second-order accuracy. The dashed line shows the variation of the error with discretization level for a vortex ring, and clearly the magnitude of the error at point 1 is always larger than for a helical vortex with finite pitch. Figure 24a shows the error behavior for point 3 with respect to the analytical solution, which is very similar to the results shown in Fig. 6b in Ref. 5. Error variation with respect to finest discretization shows a less than second-order-accurate trend.

From the results of Fig. 19a and Fig. 22a as shown previously, it is clear that the second-order error trend seen in the second method is a result of the small number of turns used in the helicoid for small M, which pushes up the error introduced by the analytic remainder. Consider the case for $p = 0.1$. When using 1000 turns, the error at $M = 10$ was found to be 1×10^{-5}, whereas in the second approach the number of turns used is 16, and the magnitude of the error was increased to 1×10^{-3}. For larger M, the magnitude of the error is smaller in the second approach because of the larger number of turns used. For point 2 (Fig. 23), the error variation is clearly second order, as indicated by a quadratic fit. The increase in the accuracy for large values of M as reported in Ref. 5 is not seen here. For larger values of helical pitch, a helix with a finite number of turns better represents the singly infinite helix. This is why the absolute error decreases with increasing helical pitch.

Accuracy of Induced-Velocity Field for a Skewed Helix

The wake of a wind turbine in yawed operation with respect to the oncoming wind resembles that of a skewed helical vortex. This skewness produces an asymmetry in the induced velocity over the plane of the turbine disk and can result in large unsteady aerodynamic loads on the blades. It is therefore important to understand the accuracy of the reconstruction of the induced velocity of a skewed helical vortex using straight-line segmentation. In this section, the accuracy of this approach is shown, and the error behavior is compared to the unskewed helix case. As in the unskewed case, the induced velocities were calculated in the $z = 0$ plane as the sum of the contribution from each vortex segment and the helical vortex was truncated at 20 turns. Errors in the calculation of the induced velocity for each discretization level were calculated with respect to the induced velocity for the finest discretization, that is, for $\Delta\theta = 0.01$ deg.

Figure 25 shows the induced velocity across the disk plane for a helical pitch of $p = 0.05$ (which is typical of wind-turbine wakes) for different skew angles. Figure 26 shows the corresponding distribution of the relative error for different skew angles. The induced velocity near $r/R = -1.2$ for the unskewed case is close to zero

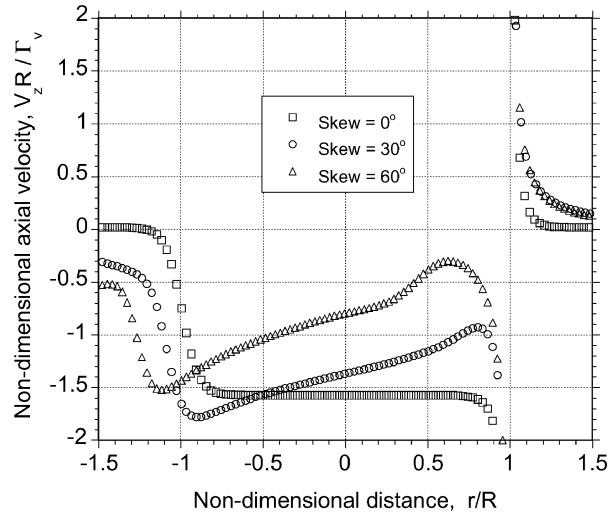

Fig. 25 Nondimensional induced axial velocity in the $z = 0$ plane of a skewed helical vortex with pitch $p = 0.05$ and skew angle $\beta = 0$, 30, and 60 deg.

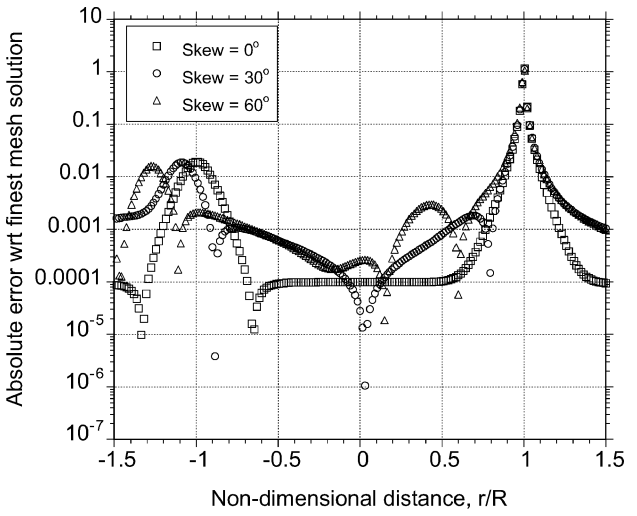

Fig. 27 Absolute error in the induced axial velocity in the $z = 0$ plane of a skewed helical vortex with pitch $p = 0.05$ and skew angle $\beta = 0$, 30, and 60 deg.

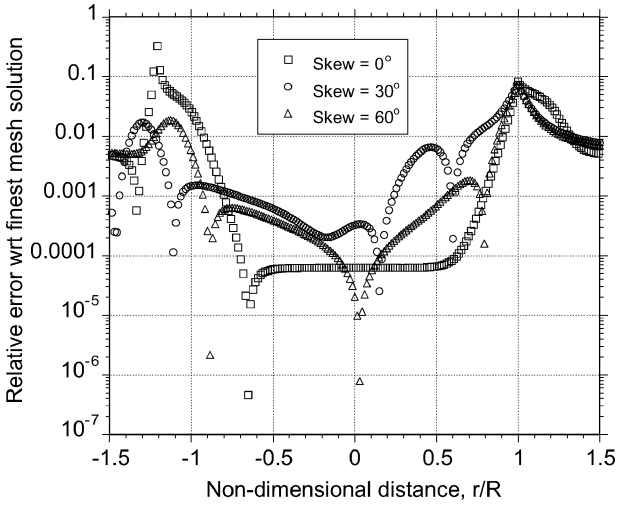

Fig. 26 Relative error in the induced axial velocity in the $z = 0$ plane of a skewed helical vortex with pitch $p = 0.05$ and skew angle $\beta = 0$, 30, and 60 deg.

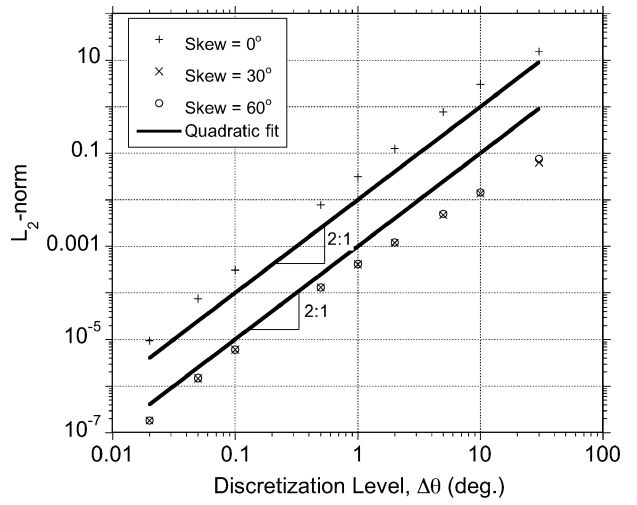

Fig. 28 L_2 norm for the relative error in the induced axial velocity in the $z = 0$ plane of a skewed helical vortex with pitch $p = 0.05$ and skew angle $\beta = 0$, 30, and 60 deg.

(see earlier), which causes an increase in the magnitude of the error. The distribution of absolute error across the $z = 0$ plane is shown in Fig. 27. Notice that the peak near $r/R = -1.2$ vanishes in this case, and the maximum error is found at the singularity ($r/R = 1.0$), which is the same as for the skewed and unskewed case. In this case there are some additional minima in the skewed case, which are a result of the cancellation of errors from adjacent turns of the helical vortex.

Figure 28 shows the convergence trend in the form of the L_2 norm calculated from the relative error. The unskewed case has relatively higher errors because of the reasons stated previously. The L_2 norm of the absolute error is plotted in Fig. 29 and these values are similar for the skewed and unskewed cases. A quadratic fit to the results for both cases again indicates the second-order accuracy of the straight-line approximation to the flowfield reconstruction.

Because it is computationally expensive to convect and track a large number of vortex filaments, the free-vortex wake models in practice use an azimuthal discretization of 5 to 20 deg for computational efficiency. (Recall that cost $\propto N_f^2$.) Figures 30 and 31 show the relative errors in the calculation of induced velocity for a practical range of azimuthal discretization of a helical vortex ($p = 0.05$, $\beta = 30$ deg). The errors are calculated with respect to a discretization of $\Delta\theta = 0.01$ deg. Figure 30 shows that at least a 10-deg

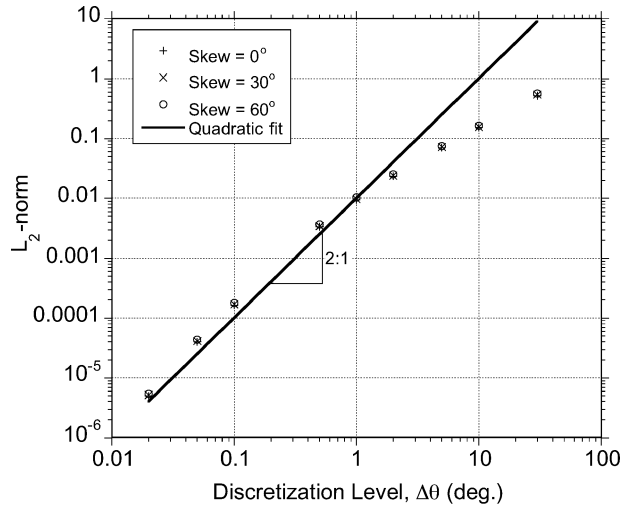

Fig. 29 L_2 norm for the absolute error in the induced axial velocity in the $z = 0$ plane of a skewed helical vortex with pitch $p = 0.05$ and skew angle $\beta = 0$, 30, and 60 deg.

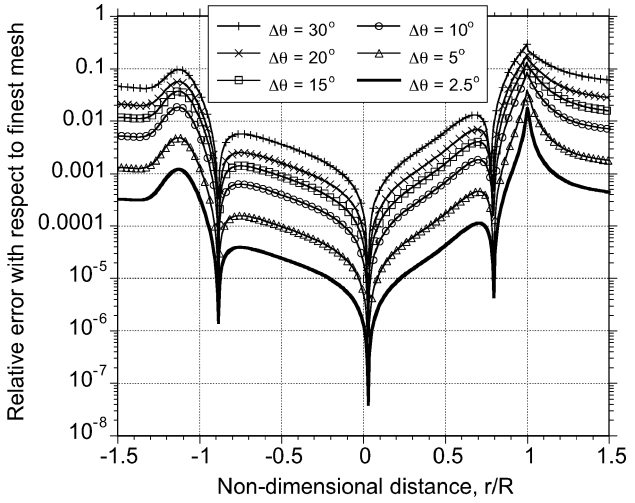

Fig. 30 Relative error distribution in the induced axial velocity in the $z = 0$ plane of a skewed helical vortex with pitch $p = 0.05$ and skew angle, $\beta = 30$ deg for practical values of $\Delta\theta$.

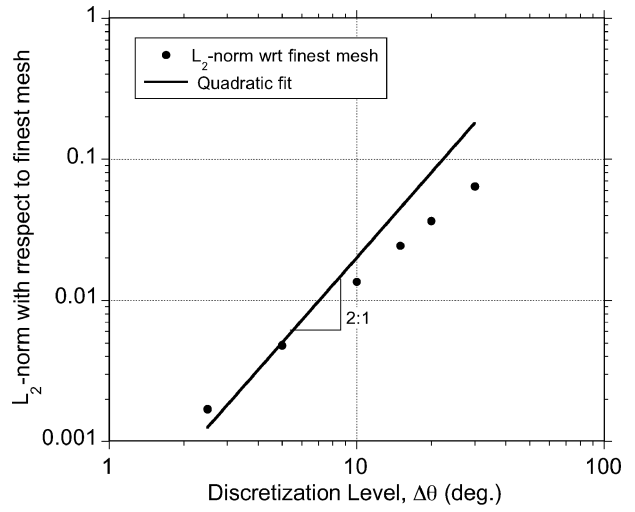

Fig. 31 Convergence trend for straight-line segmentation of a skewed helical vortex with pitch $p = 0.05$ and skew angle $\beta = 30$ deg for practical values of $\Delta\theta$.

discretization is needed to keep the magnitude of the maximum induced-velocity error below 10%. An azimuthal discretization of less than 2.5 deg is required to keep maximum error less than 1%. The accuracy of the straight-line segmentation approximation is less than second order for most practical values of $\Delta\theta$ (Fig. 31) and it is only for $\Delta\theta < 5$ deg that clean second-order accuracy is achieved.

Conclusions

A systematic study of the accuracy of the reconstruction of the induced velocity from helical vortices was performed for a range of values of helical pitch, number of turns, and wake skew angles. The purpose of this study was to evaluate the overall accuracy of the straight-line segmentation approach for use in the free-vortex wake analysis of wind-turbine aerodynamics. The following conclusions have been drawn from the results of this study:

1) The accuracy of the straight-line segmentation approach of discretizing a helical vortex is second-order for different combinations of pitch, skew, and number of turns.

2) A minimum discretization of $\Delta\theta = 10$ deg is needed to keep the maximum error in the induced velocity field less than 10%. To keep the maximum error less than 1%, a discretization of $\Delta\theta < 2.5$ deg is needed, which may be less practical for routine engineering use of vortex-wake models.

3) A vortex ring can be viewed as a special case of a helical vortex with its helical pitch tending to zero. The induced velocity from helical vortices with a helical pitch $p \to 0$ and scaled by number of turns was shown to decrease to that of a vortex ring.

4) A vortex ring was found to be a more challenging case to model accurately using the straight-line segmentation approach than the helical vortex. In the case of a vortex ring, the magnitude of the errors in the induced velocity for a particular level of discretization has been found to be larger than the corresponding helical vortex.

5) The reconstruction of induced velocity by straight-line approximation of a skewed helical vortex was also found to be second-order accurate, and the magnitude of the errors were found to be comparable to those of the unskewed case.

Acknowledgments

This work has been supported by the National Renewable Energy Laboratory in Golden, Colorado. Scott Schreck was the Technical Monitor.

References

[1]Leishman, J. G., *Principles of Helicopter Aerodynamics*, Cambridge Univ. Press, New York, 2000, Chap. 10, pp. 443–445.

[2]Bhagwat, M. J., and Leishman, J. G., "Stability, Consistency and Convergence of Time-Marching Free-Vortex Rotor Wake Algorithms," *Journal of the American Helicopter Society*, Vol. 46, No. 1, 2001, pp. 59–70.

[3]Bhagwat, M. J., and Leishman, J. G., "Accuracy of Straight-Line Segmentation Applied to Curvilinear Vortex Filaments," *Journal of the American Helicopter Society*, Vol. 46, No. 2, 2001, pp. 166.

[4]Lewis, R. I., *Vortex Element Methods for Fluid Dynamics—An Analysis of Engineering Systems*, Cambridge Univ. Press, New York, 1991, pp. 148–150.

[5]Wood, D. H., and Li, D., "Assessment of Accuracy of Representing a Helical Vortex by Straight Segments," *AIAA Journal*, Vol. 40, No. 4, 2002, pp. 647–651.

[6]Boersma, J., and Wood, D. H., "On the Self-Induced Motion of a Helical Vortex," *Journal of Fluid Mechanics*, Vol. 384, 1999, pp. 263–280.

[7]Boersma, J., and Wood, D. H., "On the Motion of Multiple Helical Vortices," *Journal of Fluid Mechanics*, Vol. 447, 2001, pp. 149–171.

[8]Leishman, J. G., Bhagwat, M. J., and Bagai, A., "Free-Vortex Filament Methods for the Analysis of Helicopter Rotor Wakes," *Journal of Aircraft*, Vol. 39, No. 5, 2002, pp. 759–775.

[9]Landgrebe, A. J., "The Wake Geometry of a Hovering Rotor and its Influence on Rotor Configurations," *Journal of the American Helicopter Society*, Vol. 17, No. 4, 1972, pp. 2–15.

[10]Kocurek, J. D., and Tangler, J. L., "A Prescribed Wake Lifting Surface Hover Performance Analysis," *Journal of the American Helicopter Society*, Vol. 22, No. 1, 1977, pp. 24–35.

[11]Robison, D. J., Coton, F. N., Galbraith, R. A. McD., and Vezza, M., "Application of a Prescribed Wake Aerodynamic Prediction Scheme to Horizontal Axis Wind Turbines in Axial Flow," *Wind Engineering*, Vol. 19, No. 1, 1995, pp. 41–51.

[12]Leishman, J. G., "Challenges in Modeling the Unsteady Aerodynamics of Wind Turbines," *Wind Energy*, Vol. 5, No. 1, 2002, pp. 85–132.

[13]Gupta, S., and Leishman, J. G., "Stability of Methods in the Free-Vortex Wake Analysis of Wind Turbines," AIAA Paper 2004-0827, Jan. 2004.

[14]Johnson, W., *Helicopter Theory*, Dover, New York, 1994, Chap. 10, pp. 540–543.

[15]Wood, D. H., "Method to Improve the Accuracy of the Straight-Segment Representation of Helical Vortices," *AIAA Journal*, Vol. 41, No. 2, 2003, pp. 256–262.

[16]Saffman, P. G., *Vortex Dynamics*, Cambridge Univ. Press, New York, 1992, Chap. 11.

S. Aggarwal
Associate Editor